www.gondwanags.org.in

Research Article

High Grade Garnet Clinopyroxene Bearing Metamorphic Sole from South-Eastern Manipur Ophiolite Belt

T. Guneshwar Singh[1*], Ibotombi Soibam[2], Kevilhoutuo Theunuo[3], Tapan Pal[4], C. Debojit Singh[3], M. Pradipkanta Singh[1] and Khetrimayum Ajit[2]

[1]*Geological Survey of India, North Eastern Region, SUMN, Imphal-795001(MN), India*
[2] *Manipur University, Chancipur, Imphal-795003(MN), India*
[3]*Geological Survey of India, Western Region, Jaipur- 302004 (RJ), India*
[4]*Formerly with Geological Survey of India*
(*Corresponding Author, E-mail: ttongbram@gmail.com)

Abstract

The reported garnet-clinopyroxene bearing metamorphic rocks occurs as metamorphic sole in the ophiolite belt of south-eastern Manipur. Textural evidences show preserved peak assemblages of grt+ cpx + amp +pl + rt ± qtz. The garnet porphyroblast have composition of ($Ca_{0.74-1}$, $Mg_{0.03-0.77}$, $Mn_{0.01-0.9}$, $Fe^{2+}_{1.2-1.6}$) ($Al_{1.90-1.98}$, $Cr_{0-0.03}$, $Fe^{3+}_{0.03-0.34}$) Si_3O_{12} and shows a progressive phase metamorphism with higher Alm_{42-52} Grs_{25-32}, $Sps_{3.66-6.91}$ and low Pyp_{12-17} at the core and lower Alm_{38-49} Grs_{24-29}, $Sps_{0.25-1.90}$ and high Pyp_{18-29} towards the rim. The high X_{Mg} (0.74-0.84) value of Clinopyroxene and negligible amount of orthopyroxene suggest a high-grade metamorphism condition. The reported garnet-clinopyroxene bearing metamorphic rock has preserved progressive metamorphic assemblages at P-T condition of 7.5 ± .50 kbar and 700-800°C. The estimated metamorphic pressures suggest a metamorphism at depths of around 25-28 km. The recorded high temperature and its mineral assemblages infer a metamorphism in a mafic granulite facies during Cenozoic continent-continent collision between Indian plate and Myanmar microplate. The intake prograde metamorphic textures with lack of prominent symplectite growth over garnet grains suggested a rapid exhumation. The exhumation history suggests a wedge exhumation along the foreland basin of the Neo-Tethyan sutures of Indo-Myanmar Ranges and is control by the presence of westerly dipping thrust that is normally out sequence to the regional thrust. Such wedge exhumation mechanism of granulite facies metamorphic sole has been reported in the central and eastern parts of Himalayas and in Kalaymyo, Myanmar, a southern extension Manipur-Nagaland ophiolite belt.

Keywords: Garnet-clinopyroxene, Metamorphic Sole, Subduction, Ophiolite, Symplectite, Out of Sequence Thrust

Introduction

Many Tethyan ophiolite are structurally underlain by thin sheets of metamorphic sole rocks (Williams and Smyth, 1973; Dilek *et al.*, 1999; Robertson, 2002). Metamorphic soles are thought to form at the inception of oceanic subduction beneath the hot sub ophiolitic mantle of the hanging wall (Jamieson, 1986). Initiation of subduction and formation of metamorphic soles have been linked to the ophiolite emplacement process (Hacker *et.al.,* 1996; Williams and Smyth, 1973). Most studies on the metamorphic evolution of metabasites in the Himalaya and Trans-Himalayan region focused on high P/T type eclogites (de Sigoyer *et al.,* 2000; Kaneko *et al.,* 2003; Parrish *et al.,* 2006; Chatterjee and Ghose, 2010) and on retrogressed eclogite overprinted by amphibolite–granulite facies metamorphism (Lombardo and Rolfo, 2000; Groppo *et al.,* 2007; Liu *et al.,* 2007; Chakungal *et al.* 2010;

Corrie *et al.,* 2010), which were formed during subduction and/or subsequent continent–continent collision. High pressure metamorphic rocks from ophiolite melanges occurs as thin dismembered thrust slices and provide significant information in understanding and reconstruction of subduction history and exhumation process (Agard *et al.,* 2009; Tsujimori and Harlow, 2012). The high-pressure eclogite and blueschist facies metamorphic rocks associated with ophiolites are reported from different parts of the Tethyan ophiolite belt of the Indian sub-continent, from Yarlung-Tsangpo Suture of Ladakh Himalayas (Groppo *et al.,* 2016) and along the Indo-Myanmar Range (IMR) from different parts of Naga Hills Ophiolite (NHO) belt (Ao and Bhowmik, 2014). On the other hand, most metabasites exposed in the Himalaya, occurring as interlayer and tectonic lenses embedded within the metapelites or granites, are normal amphibolite and granulite, not recording eclogite-facies metamorphism. The Himalaya and Trans-Himalayan is one of the best-documented examples of continent–continent collision orogenic meta-morphism. The high-grade metamorphic rocks of pelitic and felsic granulite from eastern and central part of Himalayan Orogen, have

been extensively studied, whereas mafic granulite was rarely involved (Zhang *et al.,* 2018). Mafic rocks being important constituents of the oceanic and lower continental crust, investigation into them may provide important petrological constraints for revealing the metamorphism, partial melting, rheology of the thickened lower crust and tectonic evolution of the region. (Zhang *et al.,* 2018).

The high-grade mafic metamorphic rocks, including granulite and upper amphibolite occurring in association with ophiolite suite are rarely reported from the orogenic belt of Indo-Myanmar Range. One such amphibolite-facies rocks reported in Kalaymyo, along the southern extension of Manipur -Nagaland Ophiolite belt, has been interpreted as a metamorphic sole to the ophiolite and is dated at 115-119 Ma (Zhang *et al.*, 2017). In northern part of the Naga Hills Ophiolite, evidence of HP/LT of cold Neo Tethys subduction is reported (Pradhan *et al.,* 2022; Ao, 2023). In our present study we report for the first-time high-grade garnet clinopyroxene bearing metamorphic rocks from the south-eastern part of Manipur ophiolite belt. The present work represents metamorphic characterization and its geological significances for regional correlations and establishment of the ophiolite stratigraphy in these complex terranes of ophiolite melanges. The tectono-thermal events can effectively co-relatable with subduction related structure as well as exhumation mechanism of the oceanic crust along Neo-Tethyan suture of Indo-Myanmar Ranges.

Geology of Manipur-Nagaland Ophiolite

The Manipur Ophiolite belt comprises dismembered and tectonised suite of ultramafic, mafic diabase, volcanic rocks and pelagic sediments, aligned in a linearly parallel to the regional trend of NNE-SSW to N-S direction. It forms as part of the southern extension of the Naga Hills Ophiolite (NHO) which is exposed in the eastern most part of Indian plate along Indian-Myanmar collision zone. The ophiolite is emplaced within the accretionary wedge of the supra-subduction zone (Aitchison *et al.,* 2019) where the Indian plate subducted below the Myanmar (Burmese) microplate. It separates subducted Indian-plate oceanic lithosphere associated with high-pressure metamorphic belt to the west from Jurassic to Cretaceous magmatic arc-forearc complex of Burmese plate to the east (Mitchell *et al.,* 2012). The ophiolite belt forms the northern part of the IMR and is considered to be the eastern extension of the Indus-Tsangpo Suture zone between the Asian and Indian plate (Searle *et al.,* 2007). It lies in the western margin of the Myanmar microplate and is bounded by the active Andaman subduction zone in the west and the dextral Sagaing Fault in the east. The occurrence of high pressure / low temperature (HP/LT) metamorphic rocks from the northern part of NHO as melange of tectonic blocks suggests multiple burial and exhumation cycles of Neo-Tethys in Middle-late Jurassic age (Ao and Bhowmick, 2014). The Manipur ophiolite is characterised by abyssal peridotite and cumulates as spinel lherzolites, harzburgites and dunites (Singh, 2009; Ningthoujam *et al.,* 2012; Singh *et al.,* 2017; Ao *et al.,* 2020; Khogenkumar *et al.,* 2021). It is also characterised by occurrence of chromite and chromitite bodies as pods and lenses within serpentinized dunite-peridotite units (Pal *et al.,* 2014). This ophiolite belt has an east-dipping thrust contact with the underlying flysch sediments of Disang and Barail Group of rocks in the west and is overthrust by continental metamorphic rocks of Naga Metamorphics from the east (Brunnschweller, 1966*;* Acharya, 2010, 2015).

Field Relationship

The metamorphic rocks of the south-eastern Manipur ophiolite belt can be observed in two major detached ophiolite section *viz.* Maojang-T.Khunumyang-Laisan ophiolite and Molpibung ophiolite (Fig.1-2). Along Maojang-T.Khunumyang-Laison section metamorphic assemblages occur as alternate interlayer sequence of amphibolite and serpentinized peridotite in small size imbricate structure. The metamorphic unit is overlain by serpentinized peridotite following a westerly dipping thrust sequences. Isolated bodies of the high-grade garnet clinopyroxene bearing metamorphic units also occur as lensoidals within the amphibolite as well as serpentinized peridotite (Fig.3a-b). The lensoidal bodies of garnet-clinopyroxene bearing metamorphic units occur in varying sizes from few meters to 30 m (approx.) along the strike. At particular places, the crude layering/gneissic banding in amphibolites (Fig.3c), exhibit a general trend of N 50°E with 45° south easterly dipping. These ophiolitic metamorphic rocks are also found in association of detached blocks of un-metamorphosed gabbroic rocks and thin magnesite lenses. In the western margin of this ophiolite section near Laison village, it is mainly associated with mafic and volcanic rock assemblages. The detail description of the individual litho-assemblage units of this ophiolite section is given in Fig.2a. Along Molpibung village ophiolite, the eastern part is extensively occupied by amphibolite along with lensoidal bodies of high-grade garnet-clinopyroxene bearing metamorphic of variable size. It has a sharp lithological contact with serpentinized peridotite in the west. At places the entire metamorphic unit is intruded by mafic and basic intrusive bodies (Fig. 2b). In both of these sections, the amphibolite at particular horizons are also associated with profuse garnet grains. Along the southern extension, this metamorphic unit is exposed in limited outcrop and are lack of prominent garnet grains.

At the exposed outcrop the metamorphic unit shows medium to coarse grained garnet porphyroblast which are unevenly distributed in dark green pyroxene and amphibole groundmass (Fig. 3d)*.* The metamorphic units have wider lithological extension and variation when compared with the eastern and western marginal part. However, no significant reason could be deciphered in our present study besides the differences in modal percentage of garnet from east to west and lateral lithological variation. These ophiolitic metamorphic assemblages overrides the oceanic pelagic sediments with a westerly dipping thrust along the eastern margin whereas the western part is having normal tectonic contact with Olistostromal unit. The tectonic contacts in most of the area are conceal, however in exposed outcrop it is characterised by sheared, brecciated and silicified rocks (Fig. 3e). One such examples of thick sequence of ultramafic brecciation observed in the eastern margin of this ophiolite, near Old Samdal village can be established as tectonic breccia form along a westerly dipping thrust plane. The overall structural set up of these ophiolitic metamorphic units is control by these out of sequence thrusts. Thus, in field relation the metamorphic units in these sections underlies below the serpentinized peridotite with the younger sequence towards western direction (Fig.3f).

Analytical Technique

A total of three samples from different horizons of metamorphic units representing the isolated lenses (E-1 and E-2)
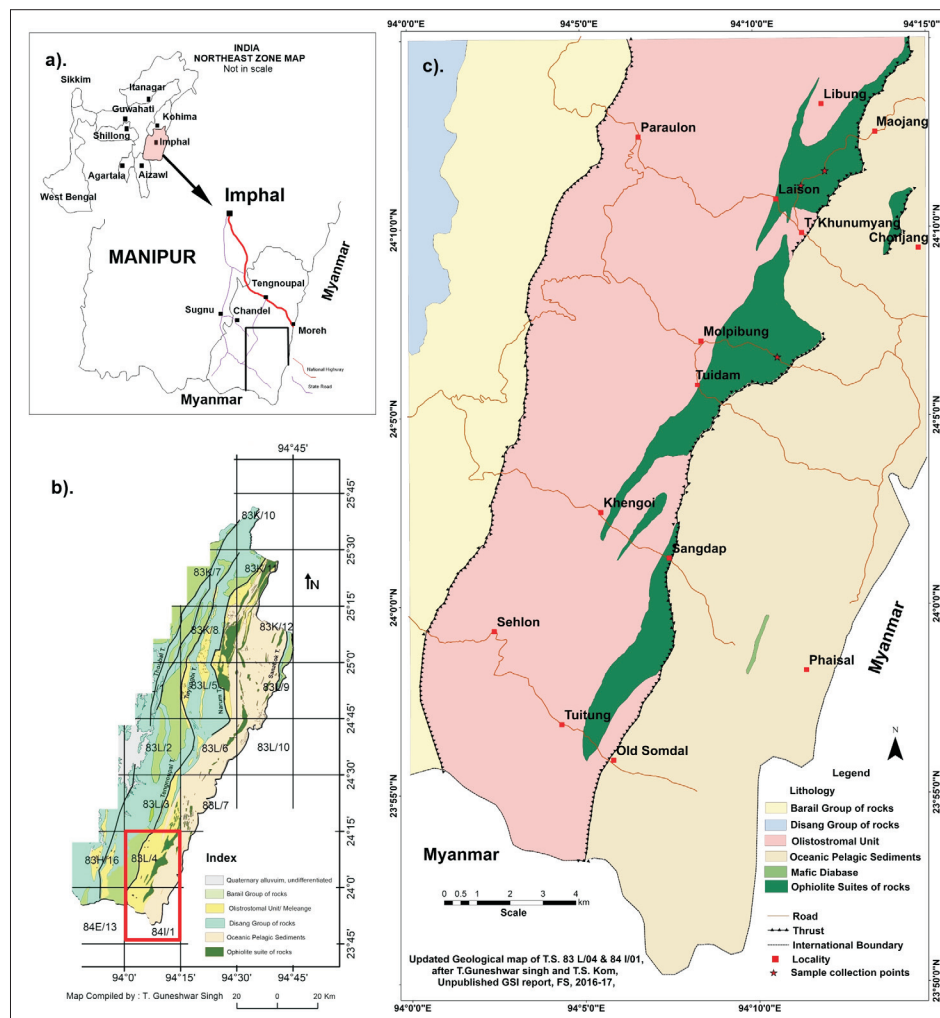
Fig.1. a) Location of Manipur, showing study area in box inset. b) Compile Geological map of Manipur Ophiolite, (compiled by T. Guneshwar Singh, sources; unpublished GSI reports) showing study area in inset box. c) Updated Geological map of extreme south eastern part of Manipur (sources from the works of Singh and Kom, 2016-17).
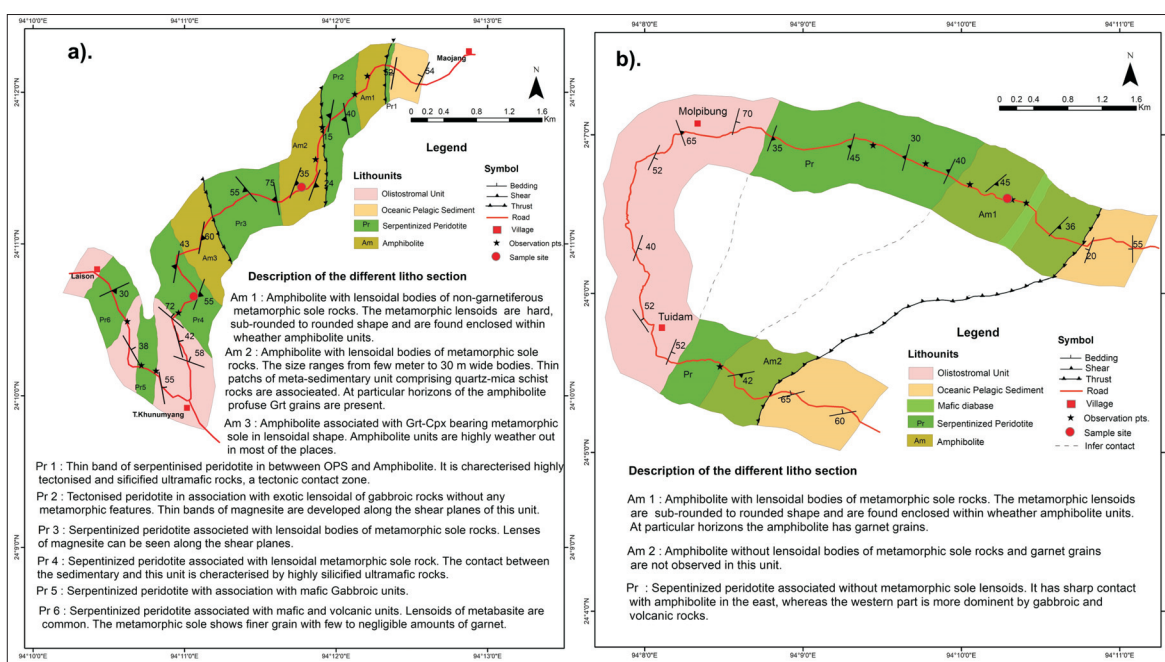
Fig.2. a) A detail geological map (1:25,000 scale) with the discription of individual litho- assemblages unit along the Maojang-T. Khunumyang-Laison village road section.
(b) A detail geological map (1:25,000 scale) with the discription of the litho-assemblages along the road section in the eastren part of Molpibung and Tuidam village.
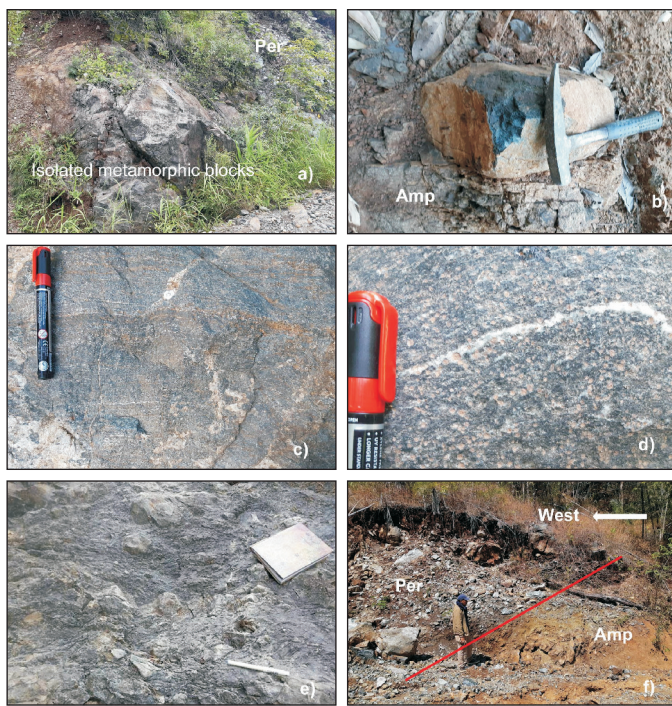
Fig.3. a) Lensoidal bodies of Grt-Cpx bearing metamorphic units within serpentinized peridotite, b) Lensoidal bodies of Grt-Cpx bearing metamorphic units in weathered Amphibolite unit, c) Crude layering in amphibolite unit of the metamorphic sole, d) Profuse garnet grains in Grt-Cpx bearing metamorphic units, e) Ultramafic brecciation in the eastern contact of ophiolite suite observed near Old Samdal village, f) Contact relation showing metamorphic unit underlying below the serpentinized peridotite in a westerly dipping plane, west of Maojang village.

and garnet bearing amphibolite (Pl-9) are analysed. Chemical composition of the these metabasites were determined with CAMECA Sx Five at EPMA Laboratory, GSI, CHQ, Kolkata. The instrument was operated with 15 kV accelerating voltage, in 1-micron beam size and 12 nA current. All-natural standards for silicate (Ca, Fe, Si, Al, Na, Mg, P, V, Ni, Cr, K, Mn, Zn and Ti) and sulphide (CuKα, CoKα, Fekα, Skα, ZnKα, AsLα, PbMα, BiMα, TaMα, AuLα, MoLα, AgLα, NiKα and SbLα) analysis were used and raw electron probe microanalysis (EPMA) data were corrected by PAP procedure (Pouchou and Pichoir, 1985). The ferric contents for all minerals are estimated from stoichiometry methods using AX software (Holland and Powell, 2006).

Petrography and Mineral chemistry

The mineral assemblage of studied metamorphic rocks comprises of garnet, hornblende, clinopyroxene, plagioclase as major mineral phase and orthopyroxene, epidote, ilmenite, rutile, titanite, quartz as accessory minerals. It dominantly exhibits well preserved garnet porphyroblast within the matrix grains of hornblende and clinopyroxene. The garnets are compositionally zoned and contain inclusions of hornblende, clinopyroxene and plagioclase. Well preserve textures of reaction rims and coronal growths around the garnet porphyroblast are visible.

Garnet porphyroblast range in size from 20 to 150 µm in diameter with inclusion of rt, ilm, plg, cpx, hbl and growth of partial coronal rimmed by Pl (Fig. 4a-b). Garnet dominantly occurs as coarse porphyroblast which suggest their formation at peak metamorphic stage. The garnet porphyroblast have composition

values of ($Ca_{0.74-1}$, $Mg_{0.03-0.77}$, $Mn_{0.01-0.9}$, $Fe^{2+}_{1.2-1.6}$) ($Al_{1.90-1.98}$, $Cr_{0-0.03}$, $Fe^{3+}_{0.03-0.34}$) Si_3O_{12}. The grains are chemically zoned and show higher values of Alm_{42-52} Grs_{25-32}, $Sps_{3.66-6.91}$ and low Pyp_{12-17} at the core and lower Alm_{38-49} Grs_{24-29}, $Sps_{0.25-1.90}$ and high Pyp_{18-29} towards the rim (Fig. 5a). The andradite composition ranges Adr_{1-11} and has slightly higher values in core (Table 1). It shows a progressive growth from core to rims. The almandine, grossular and pyrope content of the studied garnet is significantly high and low spessartine as compared to the composition of garnet in garnet-pyroxene amphibolite (Alm_{8-10} Pyp_{8-12} Grs_{09-18} Sps_{51-66}) reported from the northern part of the Naga ophiolite belt (Bhowmick and Ao, 2016).

Amphibole occurs as coarse-grained matrix associated with plagioclase, garnet and clinopyroxene, it also occurs as inclusion in garnet (Fig. 4a, d). The matrix hornblende phase occurs along with plagioclase and clinopyroxene. It has marginal contact with garnet and form as partial coronal rim along with plagioclase. In chemical composition no significant differences are observed in between the inclusion phase and matrix hornblende. However, it has slightly lower values of Ti (0.13 – 0.17) in the rims adjacent with garnet than the matrix hornblende (Table 2). The values of X_{Mg} ranges from 0.62-0.70 and falls in distinct pargasite- edenite compositional field on binary plot of Si vs $Mg/(Mg+Fe^{2+})$ (Fig. 5b). The Al-content of the hornblende varies from Al^{IV} = 1.50-1.78 with the matrix slightly lower than the rim margins having contact with garnet (Table 2).

Clinopyroxene occurs in two modes *viz.* as matrix in close association with hornblende and plagioclase often between the two
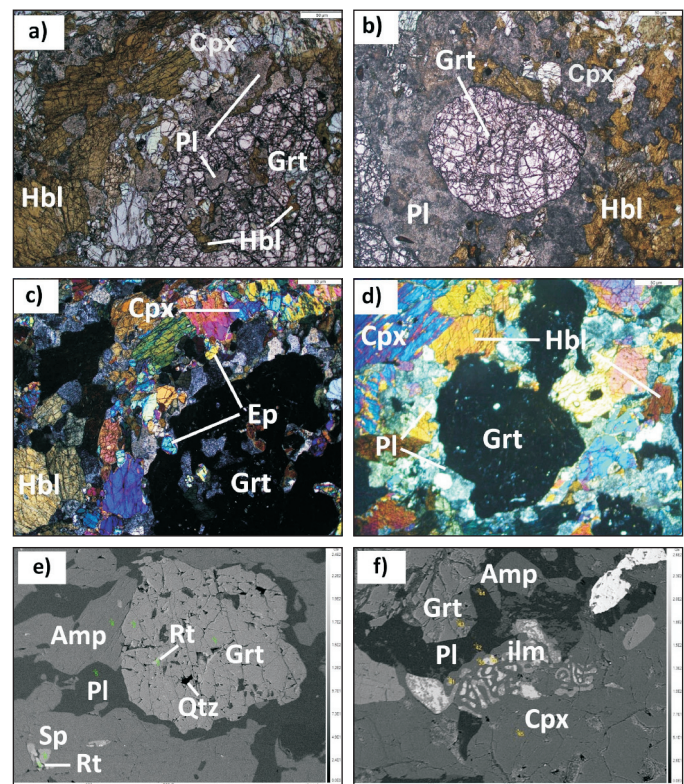
Fig. 4. a). Photomicrographs of garnet porphyroblast with inclusions of hornblende (Hbl) and plagioclase (Pl), b). Photomicrographs of garnet porphyroblast showing corona of plagioclase (Pl) along with hornblende (Hbl) and clinopyroxene (Cpx) in matrix. c). Photomicrographs of epidote grains with Cpx, Grt and Hbl in the groundmass, d). Photomicrographs of Cpx matrix, Pl and Hbl in the coronal rim of garnet grain. e). BSE image of garnet porphyroblast with inclusions of rutile (Rt), quartz (Qtz) and partial corona with amphibole and plagioclase, f). BSE image of garnet, Amp, Cpx and Pl grains and symplectite structure.

Table 1: Representative chemical analyses of garnet (stoichiometry is calculated on the basis of 12 oxygens)

Sample	E-1	E-1	E-1	E-1	E-2	E-2	E-2	E-2	E-2	E-2	Pl-9	Pl-9	Pl-9	Pl-9	Pl-9	Pl-9	Pl-9
Pts	24	25	35	43	17	18	23	24	33	34	1	8	12	15	18	21	22
Min	Grt_R	Grt_C	Grt_R	Grt_R	Grt_C	Grt_R	Grt_C	Grt_R	Grt_C	Grt_R	Grt_C	Grt_C	Grt_R	Grt_C	Grt_R	Grt_C	Grt_R
SiO_2	38.02	37.98	39.27	38.65	38.35	39.34	38.43	38.81	37.98	38.80	38.34	38.10	38.56	37.53	38.57	37.95	38.67
TiO_2	0.10	0.10	0.13	0.04	0.13	0.01	0.11	0.14	0.11	0.00	0.10	0.06	0.15	0.06	0.07	0.16	0.06
Al_2O_3	20.46	20.93	21.75	21.75	21.68	22.27	21.68	21.66	21.94	22.25	21.31	21.38	21.19	20.81	21.17	20.93	21.26
Cr_2O_3	0.54	0.00	0.05	0.10	0.02	0.01	0.08	0.05	0.19	0.06	0.00	0.00	0.02	0.06	0.02	0.00	0.00
Fe_2O_3	1.25	0.49	0.62	1.39	1.97	2.53	2.31	3.51	3.52	3.43	1.43	2.27	1.16	5.74	1.58	1.12	1.41
FeO	22.04	23.18	20.95	21.27	22.20	20.23	21.52	19.03	20.17	19.37	23.89	22.62	23.25	20.98	22.23	24.27	21.74
MnO	2.31	3.12	0.11	0.63	2.06	0.42	1.99	0.56	1.64	0.58	3.69	1.95	1.95	1.56	0.85	2.08	0.58
MgO	3.20	3.22	6.67	6.74	3.80	8.06	3.90	7.18	4.66	7.56	3.40	3.56	3.46	3.60	5.43	3.39	4.97
CaO	11.89	10.30	11.01	9.55	11.57	9.27	12.04	10.71	11.71	9.95	9.38	11.43	11.37	9.09	10.46	10.13	11.78
Na_2O	0.05	0.05	0.00	0.02	0.02	0.02	0.03	0.09	0.08	0.02	0.05	0.00	0.06	0.77	0.02	0.02	0.00
K_2O	0.00	0.00	0.00	0.00	0.00	0.02	0.00	0.00	0.00	0.04	0.00	0.01	0.00	0.24	0.00	0.01	0.00
Total	99.76	99.76	99.76	99.76	99.76	99.76	99.76	99.76	99.76	99.76	99.76	99.76	99.76	99.76	99.76	99.76	99.76
Si	2.99	3.01	3.00	2.97	2.95	2.95	2.95	2.93	2.90	2.92	2.98	2.95	2.99	2.94	2.98	2.99	2.99
Al IV	0.01	0.00	0.00	0.03	0.05	0.05	0.05	0.07	0.10	0.08	0.02	0.05	0.01	0.06	0.02	0.01	0.01
ΣY	3.00	3.00	3.00	3.00	3.00	3.00	3.00	3.00	3.00	3.00	3.00	3.00	3.00	3.00	3.00	3.00	3.00
Al VI	1.89	1.96	1.95	1.94	1.92	1.91	1.91	1.86	1.88	1.89	1.93	1.91	1.93	1.86	1.92	1.94	1.93
Al	1.90	1.95	1.96	1.97	1.97	1.97	1.96	1.93	1.98	1.97	1.95	1.95	1.94	1.92	1.93	1.94	1.94
Ti	0.01	0.01	0.01	0.00	0.01	0.00	0.01	0.01	0.01	0.00	0.01	0.00	0.01	0.00	0.00	0.01	0.00
Cr	0.03	0.00	0.00	0.01	0.00	0.00	0.01	0.00	0.01	0.00	0.00	0.00	0.00	0.00	0.00	0.00	0.00
Fe^{3+}	0.07	0.03	0.04	0.08	0.11	0.14	0.13	0.20	0.20	0.19	0.08	0.13	0.07	0.34	0.09	0.07	0.08
Fe^{2+}	1.45	1.53	1.34	1.37	1.43	1.27	1.38	1.20	1.29	1.22	1.55	1.47	1.51	1.37	1.44	1.60	1.41
Mn	0.15	0.21	0.01	0.04	0.44	0.90	0.45	0.81	0.53	0.85	0.24	0.13	0.13	0.10	0.06	0.14	0.04
Mg	0.38	0.38	0.76	0.77	0.13	0.03	0.13	0.04	0.11	0.04	0.39	0.41	0.40	0.42	0.63	0.40	0.57
Ca	1.00	0.87	0.90	0.79	0.95	0.74	0.99	0.87	0.96	0.80	0.78	0.95	0.95	0.76	0.87	0.86	0.98
Na	0.01	0.01	0.00	0.00	0.00	0.00	0.00	0.01	0.01	0.00	0.01	0.00	0.01	0.12	0.00	0.00	0.00
K	0.00	0.00	0.00	0.00	0.00	0.00	0.00	0.00	0.00	0.00	0.00	0.00	0.00	0.02	0.00	0.00	0.00
Total	8.00	8.00	8.00	8.00	8.00	8.00	8.00	8.00	8.00	8.00	8.00	8.00	8.00	8.00	8.00	8.00	8.00
XMg	0.21	0.20	0.36	0.36	0.23	0.42	0.24	0.40	0.29	0.41	0.20	0.22	0.21	0.23	0.30	0.20	0.29
Sum	3.06	3.03	3.04	3.05	3.07	3.08	3.08	3.12	3.09	3.10	3.05	3.09	3.05	3.00	3.08	3.06	3.07
Al	47.47	50.69	44.04	44.86	46.59	41.12	44.85	38.62	41.76	39.32	50.85	47.51	49.48	45.83	46.74	52.29	45.77
Py	12.29	12.56	24.95	25.34	14.22	29.21	14.49	25.97	17.19	27.34	12.90	13.31	13.12	14.02	20.33	13.02	18.62
Sp	5.03	6.91	0.23	1.35	4.37	0.88	4.19	1.16	3.43	1.19	0.25	0.00	0.29	3.91	0.00	0.10	0.00
Gross	32.79	28.88	29.62	25.83	31.11	24.15	32.14	27.83	31.05	25.89	25.57	30.75	30.99	25.43	28.16	27.98	31.74
Adr	2.42	0.96	1.15	2.63	3.72	4.64	4.32	6.42	6.57	6.26	2.72	4.28	2.23	11.28	2.96	2.16	2.64

*Alm= $(Fe2/Ca+Mg+Mn+Fe^{2+} Fe^{3+})$, Pyr = $(Mg/ Ca+Mg+ Mn+Fe^{2+} Fe^{3+})$, Sp = $(Mn/ Ca+Mg+ Mn+Fe^{2+} Fe^{3+})$, Gross = $(Ca/ Ca+Mg+ Mn+Fe^{2+} Fe^{3+})$, Adr = $(Fe3+/ Ca+Mg+ Mn+Fe^{2+} Fe^{3+})$, XMg = $(Mg/Mg+Fe^{2+})$

minerals (Fig. 4c-d), and as inclusion in garnet grains. The relict inclusion of cpx in garnet gains shows almost homogenous constituent with the core of matrix cpx. The matrix clinopyroxene grains shows reverse zoning with high Al, Fe, Ti and lower Mg values in its core and high Mg and low Al, Fe, Ti in rims (Table 3). It thus indicates that, the studied clinopyroxene grains are in prograde metamorphic phase. It shows high X_{Mg} (0.77-0.84) values and in triangular plot of Ca, Mg and Fe end-member (*after* Morimoto *et al.,* 1988), clusters in diopside field (Fig. 5c).

Plagioclase occurs in three modes *viz.* as partial coronal growth around garnet porphyroblast (Fig. 4b, d, e), inclusion in garnet and as matrix associated with clinopyroxene and amphibole (Fig. 4a). However, no significant compositional variations are observed between these grains. Plagioclases which occur as inclusion in garnet and matrix along with the clinopyroxene and amphibole are mainly albite in composition (An $_{0.62-4.22}$) and plagioclase which occurs along coronal rim around garnet porphyroblast shows slightly higher anorthite content (An $_{6.20-24.8}$) (Table 4). In triangular plots of compositional fields of plagioclase (Greenwood and Earnshaw, 1998), plagioclase (Pl) mainly falls in albite and oligoclase field (Fig. 5d).

Epidote occurs as minor phase associated with hornblende, plagioclase and clinopyroxene and as inclusion in garnet grains (Fig. 4c). It has high Al-content (23.54-27.15 wt%) and are dominantly of clinozoisite in composition. The value of Al increases in epidote with increasing temperature (Liou, 1973; Table 5).

Titanite also occurs as minor phase along the grain boundaries of clinopyroxene and often associated with epidote. It also occurs in the form of reaction rims along the grain boundary of rutile (Fig. 4e). Occurrence of rutile as accessory mineral with garnet, hornblende, plagioclase and clinopyroxene suggest possibility of high-grade condition at peak metamorphic assemblage.

Other mineral includes quartz in the form of small irregular shape crystals within garnet grains (Fig. 4e). Ilmenite occurs as minor accessary minerals along the grain boundary between garnet, plagioclase and hornblende (Fig. 4f; Table 6).

Pressure and Temperature Conditions

The P-T estimates of the progressive phase were calculated from grt-cpx thermometers. This thermometry applied to several Garnet-Cpx pairs in contact with each other yield temperatures in the ranges of 730°C to 870°C (Ganguly,1979), 665°C to 816°C (Ellis and Green,1979), 630°C to 800°C (Krogh,1988). The maximum equilibrium temperature is observed in between Grt-Cpx pairs representing rim part of the grain, whereas minimum temperature is recorded in Grt core-Cpx inclusion (Table 7).
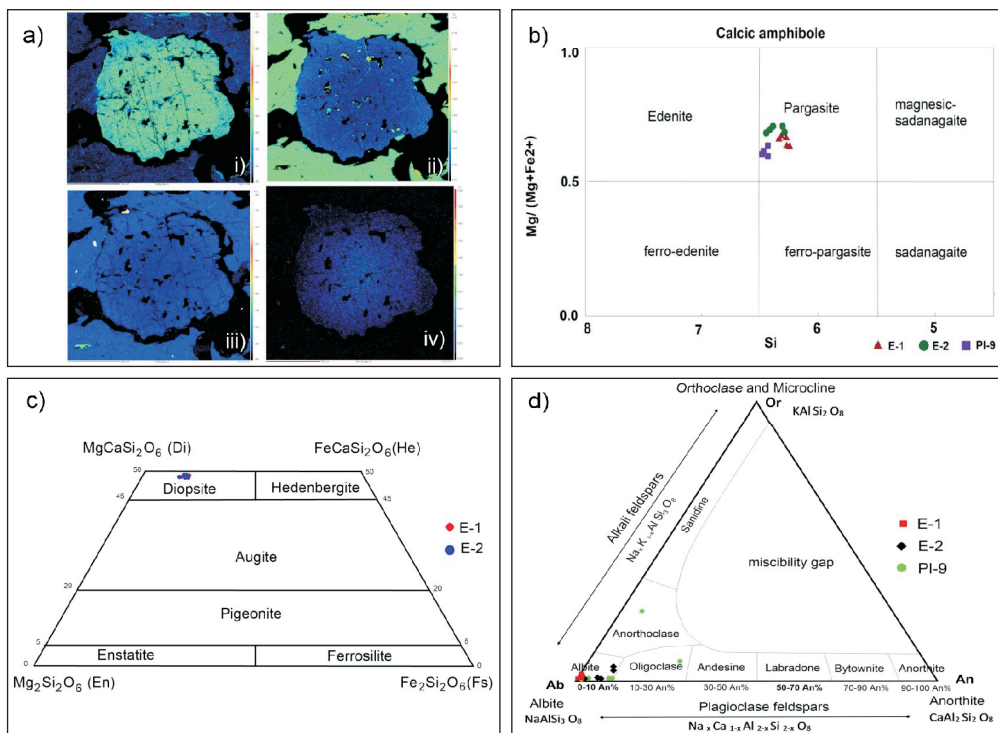
Fig.5. a) X-ray diffraction image of garnet porphyroblast showing i) compositional variation of Fe decreases towards rims, ii) composition of Mg increase towards rim, iii) compositional variation showing decrease value Ca towards rim, iv) compositional variation of Mn decreases towards rim. b) Binary plots showing the compositional fields of sodic amphiboles for the analysed samples falling in pargasite field, c) Triangular plot showing the compositional field of clinopyroxene on Ca, Mg and Fe end-member (*after* Morimoto *et al.*, 1988), d) Compositional fields of plagioclase falling in the field of albite and oligoclase on triangular plots diagram of Greenwood and Earnshaw (1998)

Table 2: Representative chemical analyses of amphibole, (stoichiometry is calculated on the basis of 23 oxygens).

Sample Mineral Points	E-1 Amp (matrix) 21	E-1 Amp matrix 30	E-1 Amp (incl) 34	E-1 Amp (adj to Grt) 37	E-1 Amp (adj to Grt) 44	E-2 Amp matrix 31	E-2 Amp (adj to Grt) 35	E-2 Amp (adj to Grt) 42	E-2 Amp matrix 48	E-2 Amp matrix 49	Pl-9 Amp (adj to Grt) 4	Pl-9 Amp (adj to Grt) 13	Pl-9 Amp matrix 19	Pl-9 Amp (adj to Grt) 23
SiO_2	42.98	42.81	42.71	42.51	41.63	44.01	42.88	42.79	44.27	43.70	43.79	43.70	43.61	43.41
TiO_2	1.94	1.89	1.72	1.98	1.50	1.72	1.50	1.33	1.66	1.68	1.26	1.19	1.41	1.51
Al_2O_3	12.84	13.01	12.84	12.99	13.35	11.76	12.75	12.91	12.32	12.04	12.95	12.72	12.56	11.95
Cr_2O_3	0.08	0.08	0.06	0.16	0.07	0.19	0.15	0.22	0.15	0.04	0.07	0.02	0.01	0.00
Fe_2O_3	1.99	2.49	2.51	2.85	3.07	1.88	3.38	3.23	2.84	2.47	3.15	3.17	3.36	2.68
FeO	11.06	10.12	10.36	9.70	10.88	10.87	9.93	10.40	10.19	10.57	11.16	11.58	11.15	12.20
MnO	0.00	0.00	0.01	0.00	0.22	0.09	0.17	0.04	0.03	0.00	0.16	0.22	0.05	0.14
MgO	12.04	12.62	12.43	12.60	11.71	12.93	12.62	12.50	13.37	12.81	11.95	11.42	11.98	11.25
CaO	11.37	11.35	11.28	11.17	11.44	11.79	11.73	11.69	11.72	11.53	11.31	11.12	11.35	11.01
Na_2O	2.26	2.35	2.36	2.28	2.43	2.17	2.06	2.25	2.20	2.08	2.01	1.87	1.82	1.99
K_2O	0.04	0.05	0.05	0.00	0.03	0.19	0.23	0.21	0.22	0.20	0.24	0.25	0.26	0.23
Total	96.49	96.68	96.31	96.17	96.12	97.60	97.40	97.56	98.96	97.12	97.88	97.02	97.31	96.15
Si	6.36	6.31	6.33	6.29	6.22	6.45	6.30	6.29	6.38	6.42	6.39	6.44	6.40	6.47
Aliv	1.64	1.69	1.67	1.71	1.78	1.56	1.70	1.71	1.62	1.58	1.61	1.57	1.60	1.53
ΣY	8.00	8.00	8.00	8.00	8.00	8.00	8.00	8.00	8.00	8.00	8.00	8.00	8.00	8.00
Al	2.24	2.26	2.24	2.27	2.35	2.03	2.21	2.24	2.09	2.09	2.23	2.21	2.17	2.10
Alvi	0.60	0.57	0.57	0.56	0.57	0.48	0.51	0.53	0.48	0.51	0.57	0.65	0.58	0.58
Ti	0.22	0.21	0.19	0.22	0.17	0.19	0.17	0.15	0.18	0.19	0.14	0.13	0.16	0.17
Cr	0.01	0.01	0.01	0.02	0.01	0.02	0.02	0.03	0.02	0.01	0.01	0.00	0.00	0.00
Fe^{3+}	0.22	0.28	0.28	0.32	0.35	0.21	0.37	0.36	0.31	0.27	0.35	0.35	0.37	0.30
Fe^{2+}	1.37	1.25	1.28	1.20	1.36	1.33	1.22	1.28	1.23	1.30	1.36	1.43	1.37	1.52
Mn	0.00	0.00	0.00	0.00	0.03	0.01	0.02	0.01	0.00	0.00	0.02	0.03	0.01	0.02
Mg	2.65	2.77	2.75	2.78	2.61	2.82	2.76	2.74	2.87	2.81	2.60	2.51	2.62	2.50
Ca	1.80	1.79	1.79	1.77	1.83	1.85	1.85	1.84	1.81	1.82	1.77	1.76	1.79	1.76
Na	0.65	0.67	0.68	0.65	0.70	0.62	0.59	0.64	0.64	0.62	0.57	0.54	0.52	0.58
K	0.01	0.01	0.01	0.00	0.01	0.04	0.04	0.04	0.04	0.04	0.05	0.05	0.05	0.04
ΣX	7.54	7.59	7.60	7.58	7.68	7.56	7.55	7.60	7.55	7.53	7.54	7.49	7.52	7.50
Total	15.54	15.59	15.60	15.58	15.68	15.63	15.68	15.72	15.66	15.62	15.54	15.49	15.52	15.50
XMg	0.66	0.69	0.68	0.70	0.66	0.68	0.69	0.68	0.70	0.68	0.66	0.64	0.66	0.62

*XMg= (Mg / Mg+Fe^{2+})

Table 3: Representative chemical analyses of clinopyroxene, (stoichiometry is calculated on the basis of 6 oxygens).

Sample	E-1	E-1	E-2	E-2	E-2	E-2	E-2	E-2	E-2
Mineral	cpx (rim)	cpx (ocre)	cpx (rim)	cpx (core)	cpx (inl)	cpx (core)	cpx (rim)	cpx (rim)	(cpx core)
Points	39	45	21	22	27	28	32	47	46
SiO_2	50.65	49.04	50.09	50.12	50.02	49.35	50.26	51.19	50.14
TiO_2	0.64	0.71	0.43	0.57	0.59	0.73	0.52	0.27	0.49
Al_2O_3	3.56	5.71	5.82	6.25	5.4	6.12	5.34	4.21	5.72
Cr_2O_3	0	0.06	0.05	0.02	0	0.1	0.1	0.04	0.07
Fe_2O_3	2.3	1.9	3.74	2.82	3.02	3.72	2.95	3.84	3.05
FeO	5.86	7.1	5.11	6.28	5.4	5.13	5.65	4.45	5.76
MnO	0.06	0.05	0.1	0.12	0	0.16	0.1	0	0.17
MgO	13.17	11.69	12.25	12.18	12.31	12.14	12.63	13.5	12.37
CaO	22.75	21.78	22.41	21.51	22.21	22.29	22.1	22.78	21.9
Na_2O	0.56	0.73	0.97	1.01	0.98	0.9	0.86	0.81	0.94
K_2O	0	0	0.01	0.03	0	0	0	0	0
Total	99.67	98.92	100.97	100.91	99.93	100.64	100.51	101.08	100.61
Si	1.89	1.85	1.84	1.85	1.86	1.83	1.86	1.88	1.85
ALIV	0.11	0.15	0.16	0.15	0.14	0.18	0.14	0.12	0.15
ΣZ	2.00	2.00	2.00	2.00	2.00	2.00	2.00	2.00	2.00
Al	0.16	0.25	0.25	0.27	0.24	0.27	0.23	0.18	0.25
ALVI	0.05	0.11	0.10	0.12	0.10	0.09	0.09	0.06	0.10
Ti	0.02	0.02	0.01	0.02	0.02	0.02	0.01	0.01	0.01
Cr	0.00	0.00	0.00	0.00	0.00	0.00	0.00	0.00	0.00
Fe^{3+}	0.07	0.05	0.10	0.08	0.08	0.10	0.08	0.11	0.09
Fe^{2+}	0.18	0.22	0.16	0.19	0.17	0.16	0.18	0.14	0.18
Mn	0.00	0.00	0.00	0.00	0.00	0.01	0.00	0.00	0.01
Mg	0.73	0.66	0.67	0.67	0.68	0.67	0.70	0.74	0.68
ΣY	1.04	1.94	1.05	1.08	1.05	1.05	1.06	1.05	1.07
Ca	0.91	0.88	0.88	0.85	0.88	0.88	0.88	0.90	0.87
Na	0.04	0.05	0.07	0.07	0.07	0.07	0.06	0.06	0.07
K	0	0	0	0.001	0	0	0	0	0
ΣX	0.95	0.93	0.95	0.92	0.96	0.95	0.94	0.95	0.93
Total	3.99	3.99	4.00	4.00	4.00	4.00	4.00	4.00	4.00
XMg	0.80	0.75	0.81	0.78	0.80	0.81	0.80	0.84	0.79

*XMg= (Mg / Mg+Fe^{2+})

Table 4: Representative chemical analyses of plagioclase, (stoichiometry is calculated on the basis of 8 oxygens).

Sample	E-1	E-1	E-1	E-1	E-2	E-2	E-2	E-2	E-2	Pl-9	Pl-9	Pl-9	Pl-9	Pl-9	Pl-9
Mineral	Fld	Fld	Fld	Fld	Fld	Fld	Fld	Fld	Fld	Fld	Fld	Fld	Fld	Fld	Fld
	matrix	matrix	matrix	rim	matrix	inl	adjgrt	adjgrt	adjgrt	adjgrt	inl	adjgrt	matrix	matrix	matrix
Point	22.00	31.00	36.00	42.00	20.00	29.00	36.00	39.00	43.00	5.00	10.00	14.00	17.00	20.00	24.00
SiO_2	67.54	67.64	67.84	66.72	68.20	66.16	66.86	67.27	66.47	60.60	66.79	59.75	68.02	67.64	67.26
TiO_2	0.00	0.02	0.00	0.06	0.02	0.00	0.00	0.00	0.00	0.00	0.00	0.00	0.00	0.01	0.00
Al_2O_3	19.38	20.06	19.85	19.99	20.01	22.12	20.88	21.05	20.77	25.32	20.87	24.67	19.27	19.32	19.39
Cr_2O_3	0.00	0.02	0.00	0.00	0.06	0.00	0.01	0.01	0.05	0.00	0.01	0.00	0.02	0.02	0.00
Fe_2O_3	0.07	0.02	0.00	0.20	0.11	0.08	0.33	0.11	0.04	0.42	0.57	0.14	0.18	0.07	0.21
FeO	0.00	0.00	0.00	0.00	0.00	0.00	0.00	0.00	0.00	0.00	0.00	0.00	0.00	0.00	0.00
MnO	0.00	0.03	0.00	0.00	0.00	0.04	0.00	0.04	0.00	0.05	0.00	0.00	0.00	0.06	0.11
MgO	0.03	0.00	0.02	0.02	0.00	0.09	0.00	0.04	0.01	0.27	0.00	0.15	0.00	0.01	0.00
CaO	0.13	0.27	0.45	1.42	0.53	1.81	1.48	1.33	1.44	1.10	2.13	5.12	0.40	0.69	0.89
Na_2O	11.53	11.44	10.92	10.84	12.00	10.18	11.07	11.35	11.08	7.01	10.35	7.47	10.71	10.81	10.96
K_2O	0.09	0.14	0.06	0.08	0.08	0.75	0.04	0.02	0.07	3.79	0.08	1.16	0.05	0.04	0.05
Total	98.76	99.97	99.23	99.33	101.01	101.23	100.67	101.22	99.93	98.52	100.77	98.58	99.02	98.87	98.88
Si	2.99	2.97	2.98	2.95	2.96	2.88	2.92	2.92	2.92	2.74	2.91	2.70	3.00	2.99	2.98
Al	1.01	1.04	1.03	1.04	1.02	1.13	1.07	1.08	1.08	1.35	1.07	1.32	1.00	1.01	1.01
Ti	0.00	0.00	0.00	0.00	0.00	0.00	0.00	0.00	0.00	0.00	0.00	0.00	0.00	0.00	0.00
Cr	0.00	0.00	0.00	0.00	0.00	0.00	0.00	0.00	0.00	0.00	0.00	0.00	0.00	0.00	0.00
Fe^{3+}	0.00	0.00	0.00	0.01	0.00	0.00	0.01	0.00	0.00	0.01	0.02	0.01	0.01	0.00	0.01
Fe^{2+}	0.00	0.00	0.00	0.00	0.00	0.00	0.00	0.00	0.00	0.00	0.00	0.00	0.00	0.00	0.00
Mn	0.00	0.00	0.00	0.00	0.00	0.00	0.00	0.00	0.00	0.00	0.00	0.00	0.00	0.00	0.00
Mg	0.00	0.00	0.00	0.00	0.00	0.01	0.00	0.00	0.00	0.02	0.00	0.01	0.00	0.00	0.00
ΣY	4.00	4.01	4.01	4.00	3.99	4.02	4.00	4.00	4.00	4.12	4.01	4.03	4.01	4.01	4.00
Ca	0.01	0.01	0.02	0.07	0.03	0.08	0.07	0.06	0.07	0.05	0.10	0.25	0.02	0.03	0.04
Na	0.99	0.97	0.93	0.93	1.01	0.86	0.94	0.96	0.94	0.61	0.88	0.65	0.92	0.93	0.94
K	0.01	0.01	0.00	0.00	0.00	0.04	0.00	0.00	0.00	0.22	0.00	0.07	0.00	0.00	0.00
ΣX	1.00	0.99	0.96	1.00	1.04	0.98	1.01	1.02	1.02	0.89	0.98	0.97	0.94	0.96	0.99
Totals	5.00	5.00	4.97	5.00	5.03	5.01	5.01	5.02	5.02	5.00	4.99	5.00	4.95	4.97	4.97
Xna	0.99	0.98	0.97	0.93	0.97	0.87	0.93	0.94	0.93	0.69	0.89	0.68	0.98	0.96	0.95
Xca	0.01	0.01	0.02	0.07	0.02	0.09	0.07	0.06	0.07	0.06	0.10	0.26	0.02	0.03	0.04
Xk	0.01	0.01	0.00	0.00	0.00	0.04	0.00	0.00	0.00	0.25	0.00	0.07	0.00	0.00	0.00

* Xna= (Na/Ca+Na+K)*100, Xca= (Ca/Ca+Na+K)*100, Xk= (K/Ca+Na+K)*100

Table 5: Representative chemical analyses of epidote, (stoichiometry is calculated on the basis of 12.5 oxygens)

Sample	Pl-9	Pl-9	E-1	E-1	E-1	E-2	E-2	E-2	E-2	E-2	E-2	E-2	E-2
Mineral	9	11	33	28	29	19	26	30	37	38	41	44	45
Point	Ep (incl)	Ep (vein)	Ep (vein)	Ep (Incl)	Ep(vein)	Ep (vein)	Ep (incl)	Ep (incl)	Ep (incl)	Ep (incl)	Ep (incl)	Ep (incl)	Ep (vein)
SiO_2	42.95	38.47	43.1	43.65	43.31	43.78	43.61	38.02	39.02	45.75	35.85	37.92	43.52
TiO_2	0.01	0.21	0.04	0	0.04	0.00	0.00	0.08	0.13	0.00	0.05	0.00	0.03
Al_2O_3	21.22	27.13	22.96	23.42	22.75	24.96	24.08	27.15	26.74	23.95	25.75	26.74	23.54
Cr_2O_3	0	0	0	0.02	0.04	0.02	0.00	0.00	0.00	0.02	0.04	0.04	0.00
$Fe_2O_3$3	0.36	0.84	0.08	0.04	0.08	0.00	0.00	0.00	0.00	0.00	0.00	0.00	0.00
FeO	2.85	6.72	0.68	0.35	0.62	0.72	1.11	1.99	2.58	0.32	3.56	2.09	1.56
MnO	0.01	0	0.07	0	0	0.03	0.03	0.07	0.16	0.02	0.04	0.11	0.00
MgO	0	0.08	0	0.02	0.01	0.20	0.00	2.43	1.98	0.03	2.32	2.14	0.00
CaO	26.51	23.95	26.44	26.14	26.25	25.78	27.31	23.30	22.38	25.66	23.50	22.81	27.89
Na_2O	0.03	0.02	0.08	0.1	0.17	0.50	0.07	0.20	0.82	0.76	0.06	0.27	0.03
K_2O	0.02	0	0	0.02	0.02	0.00	0.01	0.11	0.03	0.01	0.00	0.02	0.02
Total	94.15	97.74	93.74	94.05	93.55	95.99	96.22	93.35	93.84	96.52	91.17	92.14	96.61
Si	3.47	3.05	3.45	3.47	3.47	3.404	3.405	3.071	3.135	3.520	3.006	3.100	3.401
Al	2.02	2.54	2.17	2.20	2.15	2.288	2.217	2.585	2.533	2.173	2.546	2.577	2.168
Aliv	2.00	2.00	2.00	2.00	2.00	2.00	2.00	2.00	2.00	2.00	2.00	2.00	2.00
Fe^{3+}	0.02	0.05	0.17	0.20	0.15	0.288	0.217	0.585	0.533	0.173	0.546	0.577	0.168
Alvi	0.02	0.54	0.01	0.00	0.00	0.000	0.000	0.000	0.000	0.000	0.000	0.000	0.000
Fe^{3+}Alvi	0.04	0.59	0.17	0.20	0.16	0.288	0.217	0.585	0.533	0.173	0.546	0.577	0.168
Ti	0.00	0.01	0.00	0.00	0.00	0.000	0.000	0.005	0.008	0.000	0.003	0.000	0.002
Cr	0.00	0.00	0.00	0.00	0.00	0.001	0.000	0.000	0.000	0.001	0.003	0.003	0.000
Fe^{2+}	0.19	0.45	0.05	0.02	0.04	0.047	0.072	0.134	0.173	0.021	0.250	0.143	0.102
Mn	0.00	0.00	0.00	0.00	0.00	0.023	0.000	0.293	0.237	0.003	0.290	0.261	0.002
Mg	0.00	0.01	0.00	0.00	0.00	0.002	0.002	0.005	0.011	0.001	0.003	0.008	0.000
Ca	2.30	2.04	2.27	2.23	2.26	2.148	2.285	2.017	1.927	2.116	2.112	1.998	2.335
Na	0.00	0.00	0.01	0.02	0.03	0.075	0.011	0.031	0.128	0.113	0.010	0.043	0.005
K	0.00	0.00	0.00	0.00	0.00	0.000	0.001	0.011	0.003	0.001	0.000	0.002	0.002
Totals	8.01	8.14	7.96	7.94	7.96	7.989	7.992	8.153	8.156	7.95	8.221	8.133	8.017
XMg	0.00	0.02	0.00	0.09	0.03	0.33	0.00	0.69	0.58	0.13	0.54	0.65	0.02

*XMg = (Mg/ Mg + Fe^{2+})

Table 6: Representative chemical analyses of Rt, Ttn and Ilm, (stoichiometry is calculated on the basis of 2 oxygen for Rt, 5 for Ttn and 3 for Ilm).

Sample	Pl-9	Pl-9	Pl-9	E-1	Pl-9	E-1	E-1	E-1	E-1	E-2	E-2	E-1	E-1
Mineral	Rt	Rt	Rt	Rt	Ttn	Ttn	Ttn	Ttn	Ttn	Ttn	Ttn	ilm	ilm
Point	7	3	16	26	6	23	32	38	41	25	40	27	40
SiO_2	0.05	0	0	0.04	30.11	30.23	29.6	30	28.4	30.12	30.35	0.04	0.13
TiO_2	98.13	98.71	99.31	97.58	38.18	38.31	37.37	38.39	42.12	38.52	39.14	49.33	47.01
Al_2O_3	0.08	0.01	0.02	0.02	1.31	1.2	1.39	1.1	0.42	1.33	1.14	0.05	0.03
Cr_2O_3	0.05	0	0.07	0.16	0	0	0	0.01	0	0	0.02	0.09	0.19
Fe_2O_3	0.06	0.08	0.06	0.09	0.08	0.06	0.07	0.06	0.06	0.11	0.07	4.92	4.73
FeO	0.50	0.61	0.51	0.72	0.65	0.45	0.59	0.48	0.50	0.86	0.61	39.7	38.18
MnO	0	0	0	0	0.1	0.2	0.15	0	0.04	0.19	0	3.95	4.3
MgO	0	0.03	0	0.03	0.06	0.02	0.17	0.03	0	0	0.05	0	0.06
CaO	0.41	0.25	0.14	0.27	28.72	28.27	27.73	27.82	26.81	29.02	29.08	0.39	0.63
Na_2O	0	0	0	0	0	0	0.05	0	0.06	0.01	0.02	0.03	0.13
K_2O	0	0	0	0.01	0	0.01	0	0	0	0.01	0	0.01	0
Total	99.33	99.7	100.16	98.92	99.68	99.44	97.82	98.26	98.63	100.7	101.08	98.28	94.93
Si	0.00	0.00	0.00	0.00	0.60	0.60	0.60	0.60	0.57	0.59	0.59	0.00	0.00
Ti	1.49	1.49	1.49	1.49	0.57	0.57	0.57	0.58	0.63	0.57	0.58	0.95	0.94
Al	0.00	0.00	0.00	0.00	0.03	0.03	0.03	0.03	0.01	0.03	0.03	0.00	0.00
Cr	0.00	0.00	0.00	0.00	0.00	0.00	0.00	0.00	0.00	0.00	0.00	0.00	0.00
Fe^{3+}	0.00	0.00	0.00	0.00	0.00	0.00	0.00	0.00	0.00	0.00	0.00	0.09	0.09
Fe^{2+}	0.01	0.01	0.01	0.01	0.01	0.01	0.01	0.01	0.01	0.01	0.01	0.85	0.85
Mn	0.00	0.00	0.00	0.00	0.00	0.00	0.00	0.00	0.00	0.00	0.00	0.09	0.10
Mg	0.00	0.00	0.00	0.00	0.00	0.00	0.01	0.00	0.00	0.00	0.00	0.00	0.00
Ca	0.01	0.01	0.00	0.01	0.61	0.60	0.60	0.60	0.57	0.61	0.61	0.01	0.02
Na	0.00	0.00	0.00	0.00	0.00	0.00	0.00	0.00	0.00	0.00	0.00	0.00	0.01
Totals	1.51	1.51	1.51	1.51	1.82	1.81	1.82	1.81	1.80	1.82	1.82	2.00	2.01

Temperature conditions at the time of metamorphism for the metamorphic sole rocks were also calculated using the hornblende-plagioclase thermobarometry of Holland and Blundy (1994). This thermobarometry was applied to several adjacent pairs of amphibole and plagioclase in contact with each other and yield temperatures ranging from 665°C-713°C (Holland and Blundy, 1994), 665°C-746°C (Holland and Blundy, 1994) at pressure 6.95-8.13 kbar (Schmidt, 1992) and 663°C -712°C

Table 7: Geo-thermometry of Grt-Cpx mineral pair, after Ganguly (1979), Ellis and Green (1979), Krogh (1988)

Slide No.	E-2	E-2	E-2	E-2	E-2	E-2	E-2	E-2	E-2
Rock type	Metabasites	Metabasites	Metabasites	Metabasites	Metabasites	Metabasites	Metabasites	Metabasites	Metabasites
Sample No.	grt33,cpx46	grt34, cpx24	grt33,cpx27	grt33,cpx28	grt34,cpx32	grt23,cpx27	grt43, cpx39	grt24,cpx21	grt23, cpx22
Textural specification	core-core	rim-rim	core-incl	core-core	rim-rim	core-incl	rim-rim	rim-rim	core-core
$Fe^{+2}(24O_2)Gt$	2.58	2.44	2.58	2.58	2.44	2.76	2.73	2.41	2.76
$Mg(24O_2)Gt$	1.06	1.69	1.06	1.06	1.69	0.89	1.54	1.62	0.89
$Ca(24O_2)Gt$	1.92	1.60	1.92	1.92	1.60	1.98	1.57	1.73	1.98
$Mn(24O_2)Gt$	0.21	0.07	0.21	0.21	0.07	0.26	0.08	0.07	0.26
$Fe^{+2}(12O_2)Gt$	1.29	1.22	1.29	1.29	1.22	1.38	1.37	1.20	1.38
$Mg(12O_2)Gt$	0.53	0.85	0.53	0.53	0.85	0.45	0.77	0.81	0.45
$Ca(12O_2)Gt$	0.96	0.80	0.96	0.96	0.80	0.99	0.79	0.87	0.99
$Mn(12O_2)Gt$	0.11	0.04	0.11	0.11	0.04	0.13	0.04	0.04	0.13
XCaGt	0.33	0.28	0.33	0.33	0.28	0.34	0.27	0.30	0.34
$XFe^{+2}Gt$	0.45	0.42	0.45	0.45	0.42	0.47	0.46	0.41	0.47
XMnGt	0.04	0.01	0.04	0.04	0.01	0.04	0.01	0.01	0.04
XMgGt	0.18	0.29	0.18	0.18	0.29	0.15	0.26	0.28	0.15
$Fe^{+2}(6O_2)Cpx.$	0.18	0.14	0.17	0.16	0.18	0.17	0.18	0.16	0.19
$Mg(6O_2)Cpx.$	0.68	0.74	0.68	0.67	0.70	0.68	0.73	0.67	0.67
$Mn(6O_2)Cpx$	0.01	0.00	0.00	0.01	0.00	0.00	0.00	0.00	0.00
$XFe^{+2}Cpx$	0.21	0.16	0.20	0.19	0.20	0.20	0.20	0.19	0.22
XMgCpx	0.79	0.84	0.80	0.80	0.80	0.80	0.80	0.81	0.77
(ln Kd)	2.23	2.05	2.29	2.32	1.74	2.53	1.96	1.85	2.37
P(in KBar)	8	8	8	8	8	8	8	8	8
T(C) (Ganguly,1979)	786.24	800.73	774.20	767.07	870.43	730.39	816.78	851.78	760.28
T(C) (Ellis & Green,1979)	730.86	732.90	716.66	708.28	816.58	665.00	746.98	803.21	699.65
T(C) (Krogh,1988)	702.17	705.10	686.46	677.22	799.71	629.49	719.66	785.36	667.35

(Holland and Blundy, 1994) at pressure 6.96-7.90 kbar (Anderson and Smith, 1995). Temperature recorded based on Ti content in amphibole (Otten, 1984) ranges from 703°C-809°C. Slightly higher pressure and temperature are recorded in the rim pairs (8.13 kbar and 744°C) then the matrix pairs (6.95 kbar and 665°C) (Table 8).

A strong correlation between increasing Al contents of amphiboles and increasing pressure makes it possible to use an Al-in-amphibole barometer (Hammarstrom and Zen, 1986; Hollister *et al.,* 1987; Johnson and Rutherford, 1989; Schmidt, 1992). Applying this geobarometer, the Al content in hornblende yielded a pressure range from 6.92 to 8.17 kbar (Schmidt, 1992). Slightly higher pressure is recorded in the rim parts then the matrix hornblende grains (Table 9).

Metamorphic History

The bulk mineral assemblages of garnet, clinopyroxene, amphibole and plagioclase with negligible pervasive foliation, suggest the original protolith could be of mafic rocks. Textural evidences and mineralogical composition indicate that the studied garnet-clinopyroxene bearing metamorphic units evolved through progressive phase metamorphic mineral reconstitution. The prograde reaction history is best constrained by the inclusion assemblage of hornblende + plagioclase + ilmenite ± quartz within garnet and clinopyroxene grains. The peak mineral assemblage can be given as garnet + clinopyroxene + hornblende + plagioclase + rutile ± quartz.

The garnet grains having inclusion of clinopyroxene and plagioclase mineral phase can be established by the following progressive metamorphic reaction (i).

$$cpx + pl = grt \qquad (i)$$

Garnet porphyroblast can also formed by consumption of plagioclase and amphibole. With subsequent incongruent melting of plagioclase and Ca-amphibole produces cpx and melt (Wolf and Wyllie, 1993). Thus, the peak metamorphic reaction can be represented by the following metamorphic reaction (ii).

$$pl + hbl + ilm = grt + cpx + rt + H_2O \qquad (ii)$$
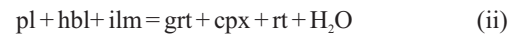
with progressive metamorphism at sub-solidus pressure and temperature, when plagioclase is consumed by reaction with Ca-amphibole (Ernst and Liu, 1998) it gives the reaction (iii).

$$pl + prg = grt + ed ± qtz \ (P=1.2\text{-}1.4 \ GPa/T=800°C) \qquad (iii)$$
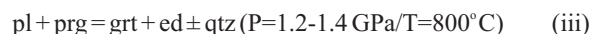
The composition of Ca-amphibole falling in pargasite-edenite field and the textural preservation of Ca-rich grossular garnet porphyroblast having pargasite, oligoclase and rutile as inclusion can be explained by the above reaction. However, in present mineral assemblage the composition of edenite is at initial stage of formation without any coarse-grained quartz phenocryst, suggesting that exhumation or decompression must have occurred prior to the completion of this reaction.

The mineral texture for retrograde metamorphism in the study samples is negligible except for few vermicular growths of ilmenite + titanite within the clinopyroxene grains. The growth of titanite rims in ilmenite/rutile and epidote minerals phase suggested a mineral reconstitution at lower P/T retrogression phase during exhumation.

Discussion

The metamorphic mineral assemblages and preserved reaction textures provide a progressive stage metamorphism in a precursor rock of gabbroic and basaltic oceanic crust at the time of subduction and obduction of the Indian plate and Myanmar microplate. The petrological studies show no significant differences in between the samples of isolated metamorphic lensoids and garnet bearing amphibolite. It is therefore, the isolated metamorphic lensoids can be inferred as scrap up blocks from the part of

Table 8: Plagioclase-Hornblende Thermobarometry temperature by Holland and Blundy, (1994), at pressure by Schmidt (1992) and Anderson and Smith (1995)

Sample	Pl-9	Pl-9	Pl-9	Pl-9	E-1	E-1	E-1	E-1	E-2	E-2
Mineral	Amp	Amp	Amp	Amp	Amp C	Amp	Amp	Amp	Amp	Amp
Point no.	4	13	19	23	21	30	37	44	35	42
SiO_2	43.79	43.7	43.61	43.41	42.93	42.81	42.51	41.63	42.88	42.79
TiO_2	1.26	1.19	1.41	1.51	1.94	1.89	1.98	1.5	1.5	1.33
Al_2O_3	12.95	12.72	12.56	11.95	12.84	13.01	12.99	13.35	12.75	12.91
FeO*	14	14.43	14.18	14.62	12.85	12.36	12.27	13.64	12.97	13.3
MgO	11.95	11.42	11.98	11.25	12.04	12.62	12.6	11.71	12.62	12.5
MnO	0.16	0.22	0.05	0.14	0	0	0	0.22	0.17	0.04
CaO	11.31	11.12	11.35	11.01	11.37	11.35	11.17	11.44	11.73	11.69
Na_2O	2.01	1.87	1.82	1.99	2.26	2.35	2.28	2.43	2.06	2.25
K_2O	0.24	0.25	0.26	0.23	0.04	0.05	0.06	0.03	0.23	0.21
Sum	97.67	96.92	97.22	96.11	96.27	96.44	95.86	95.95	96.91	97.02
Formula per Holland and Blundy, 1994										
Si	6.37	6.42	6.38	6.45	6.33	6.29	6.27	6.20	6.28	6.28
Aliv	1.63	1.58	1.62	1.55	1.67	1.71	1.73	1.80	1.72	1.72
Al(total)	2.22	2.20	2.17	2.09	2.23	2.25	2.26	2.34	2.20	2.23
Alvi	0.60	0.62	0.54	0.54	0.57	0.54	0.53	0.54	0.49	0.51
Ti	0.14	0.13	0.16	0.17	0.22	0.21	0.22	0.17	0.17	0.15
Fe^{3+}	0.52	0.52	0.55	0.48	0.40	0.45	0.48	0.52	0.54	0.52
Mg	2.59	2.50	2.61	2.49	2.65	2.76	2.77	2.60	2.76	2.73
Mn	0.02	0.03	0.01	0.02	0.00	0.00	0.00	0.03	0.02	0.00
Fe^{2+}	1.14	1.20	1.14	1.30	1.18	1.04	0.99	1.15	1.03	1.08
Ca	0	0	0	0	0	0	0	0	0	0
Sum	5	5	5	5	5	5	5	5	5	5
Fe	0.05	0.05	0.05	0.04	0.01	0.03	0.04	0.03	0.02	0.02
Ca	1.76	1.75	1.78	1.75	1.80	1.79	1.77	1.82	1.84	1.84
Na	0.19	0.20	0.17	0.21	0.19	0.19	0.20	0.15	0.14	0.14
Sum	2	2	2	2	2	2	2	2	2	2
Ca	0	0	0	0	0	0	0	0	0	0
Na	0.38	0.33	0.35	0.36	0.46	0.48	0.46	0.55	0.45	0.50
K	0.04	0.05	0.05	0.04	0.01	0.01	0.01	0.01	0.04	0.04
Sum	0.42	0.38	0.39	0.41	0.46	0.49	0.47	0.56	0.49	0.54
mineral	Pl	Pl	Pl	Pl	Pl R	Pl	Pl	Pl	Pl	Pl
Point no.	5	14	20	24	22	31	36	42	36	43
XAb	0.69	0.68	0.96	0.95	0.99	0.98	0.97	0.93	0.93	0.93
X An	0.06	0.26	0.03	0.04	0.01	0.01	0.02	0.07	0.07	0.07
Results based on Schmidt pressure (used for purposes of calculation)										
Pschmidt (kb)	7.57	7.47	7.30	6.95	7.62	7.71	7.75	8.14	7.48	7.62
T (C) HB1 '94	713.18	707.30	672.93	663.27	665.91	675.57	683.62	689.91	695.20	686.59
T (C) BH '90	746.94	744.57	688.97	682.82	687.89	696.50	699.43	716.73	709.92	709.58
Results based on iteration using Anderson and Smith pressure at various thermometers										
T (C) HB1'94	712.33	706.31	672.93	663.25	665.98	675.58	683.67	689.98	695.74	686.80
P(Kb) HB1'94	6.96	6.98	7.33	7.10	7.74	7.70	7.62	7.91	7.16	7.44
Temperature based on Ti (Otten, 1984)										
T (C) Ti-hbld	711.05	703.23	731.72	748.14	804.13	796.33	809.57	747.14	744.07	721.62

metamorphic sole rocks. The high percent of almandine and grossular in garnet suggested an intermediate to high grade metamorphism in regionally or thermally influence environment. The zoning of Garnet with Mn rich cores and Mg rich rims suggest growth from lower P/T condition to higher P/T condition *i.e.* prograde metamorphism involving increasing temperature and pressure. The high ($X_{Mg77-84}$) values of clinopyroxene and negligible amount of orthopyroxene confirm a high-grade metamorphism.

The metamorphic P/T condition of the studied samples are calculated by the used of grt-cpx geothermometer (Ganguly, 1979; Ellis and Green, 1979; Krogh, 1988), hbl-plg thermobarometry (Holland and Blundy, 1994, at pressure by Schmidt, 1992) and Al-in-amphibole barometer (Schmidt, 1992). The temperature dependence of Mg- Fe^{2+} exchange between garnet and clinopyroxene has long been recognized as a potential

Table 9: Al in hornblende barometer of Schmidt (1992)

Sample No.	Mineral points	Al_{total}	Pressure (kbar)
E-1	21 (matrix)	2.239	7.64764
E-1	30 (matrix)	2.26	7.7476
E-1	34 (incl.)	2.243	7.66668
E-1	37 (rim)	2.266	7.77616
E-1	44 (rim)	2.35	8.176
E-2	31 (matrix)	2.030	6.6528
E-2	35 (rim)	2.209	7.50484
E-2	42 (rim)	2.237	7.63812
E-2	48 (matrix)	2.094	6.95744
E-2	49 (matrix)	2.086	6.91936
Pl-9	4 (rim)	2.229	7.60004
Pl-9	13 (rim)	2.213	7.52388
Pl-9	19 (matrix)	2.174	7.33824
Pl-9	23 (rim)	2.101	6.99076

Values based on Al total vs (Fe^{2+}/Fe^{2+} + Mg)

geothermometer (Mysen and Heier, 1972; Ellis and Green, 1979; Ganguly, 1979; Krogh, 1988; Raheim and Green, 1974*).* The hornblende-plagioclase thermobarometry performs well (±40°C) in the temperature range 400-1000°C and pressure of 1-15 kbar (Holland and Blundy, 1994, at pressure by Schmidt, 1992; Anderson and Smith, 1995). As quartz is negligible in the assemblage, the edenite -richterite thermometer was used in the formula. The metamorphic P/T deduced from the adjacent pairs of grt-cpx and hbl-plg does not give significant differences between core and rim parts. As a result, average pressure-temperature (*P-T*) conditions of $7.5 \pm .50$kbar and ranges of 700° to 800°C were estimated for the analysed metamorphic unit. The appearance of garnet and clinopyroxene under relatively high temperature and moderate P conditions (*e.g.* 7 kbar at $700\sim800^{\circ}$C) is consistent with the results obtained from high–pressure experiments on quartz-tholeiite (Green and Ringwood, 1967). The estimated metamorphic pressures suggest a metamorphism at depths of around 25-28km.

The field relation showing metamorphic unit underling below the serpentinized peridotite in a westerly dipping stratigraphic sequence, confronts a typical nature of a metamorphic sole. The studied metamorphic units which occur as interlayer and tectonic lenses embedded within amphibolite and serpentinized peridotite are represented by normal amphibolite and mafic granulite. The preserved/intake prograde metaphoric textures with lack of prominent symplectite growth over garnet grains suggested a rapid exhumation. The mineral foliation observed in amphibolite unit suggested that, metamorphism events may have taken place in a different tectonic event. It is logical to infer that, the metamorphism has occurred during Cenozoic continent-continent collision that leads to obduction of the oceanic crust from the hanging wall of the subducting plate. Exhumation of these metamorphic units is further exaggerated by westerly dipping out of thrust sequences. Thus, the exhumation mechanism suggests a wedge exhumation along the foreland basin of the Neo-Tethyan sutures of Indo-Myanmar Ranges and is control by the westerly dipping thrust that is normally out sequence to the regional thrust. Such wedge exhumation due to the presence of out of thrust sequence has been explain for the metamorphic sole rocks of Kalaymyo, in the southern extension this ophiolite belt (Zhang *et al.*, 2017).

The complexities of subduction processes and metamorphism of this region cannot be deciphered with the present limited data. A more detail work on structural analyses and systematic petrological studies in future on this reported metamorphic sole will provide robust and critical information on nature of collision and understanding the tectono-event history of the Neo-Tethyan suture zones of Indo-Myanmar ranges.

Conclusions

The studied metamorphic unit represents a typical metamorphic sole, with the metamorphic unit lying below the serpentinized peridotite in a westerly dipping stratigraphic sequence due to the presence of out of thrust sequence. The ophiolite stratigraphy can be established with the younger sequences lying towards the western part of the area. The bulk mineral assemblages of garnet, clinopyroxene, amphibole and plagioclase with negligible pervasive foliation, suggest the original protolith could be of mafic rocks. It has preserved/intake progressive metamorphic texture with lack of prominent symplectite mineral growths. The peak metamorphic assemblage is represented by garnet + clinopyroxene + hornblende + plagioclase + rutile ± quartz. The reported metamorphic sole has estimated P-T condition of $7.5 \pm .50$ kbar and 700-800°C. The recorded high temperature and its mineral assemblages infer a high-grade metamorphism in a mafic granulite facies.

Authors' Contributions

TGS: Writing-Original Draft of Manuscript, Investigation and Mapping, Software, Data Analyses and Interpretation. **SI:** Conceptualization, Visualization, Methodology, Editing. **KT:** Data Analyses, Software, Writing- Original Draft of Manuscript. **TP:** Conceptualization, Visualization, Supervision, Editing. **CDS:** Supervision, Conceptualization, Reviewing and Editing. **MPS:** Investigation and Mapping, Software. **AK:** Data Analyses and Software.

Conflict of Interest

The authors declare that they have no known competing financial interests or personal relationships that could have appeared to influence the work reported in this paper.

Acknowledgements

References

Acharyya, S.K. (2010). Tectonic Evolution of Indo-Burma Range with special Reference to Naga-Manipur Hills. Mem. Geol. Soc. India, v. 75, pp. 25-43.

Acharyya, S.K. (2015). Indo-Burma Range: a belt of accreted microcontinents, ophiolites and Mesozoic-Paleogeneflyschoid sediments. Int. Jour. Earth Sci., v. 104, pp.1235-1251.

Agard, P., Yamato, P., Jolivet, L. and Burov, E. (2009). Exhumation of oceanic blueschists and eclogites in subduction zones: Timing and mechanisms. Earth-Sci. Rev., v. 92, pp. 53-79.

Aitchison, J.C., Ao, A., Bhowmik, S., Clarke, G.L., Ireland, T.R., Kachovich, S. and Zhen, Y. (2019). Tectonic evolution of the western margin of the Burma microplate based on new fossil and radiometric age constraints. Tectonics, v. 38(5), pp. 1718-1741.

Anderson, J.L. and Smith, M.W. (1995). The effects of temperature and 102 on the Al-in-hornblende barometer. Am. Mineralog., v. 80, pp. 549-559.

Ao, A. (2023). Tectonic slices of greenschist - epidote blueschist - epidote amphibole schist - garnet epidote amphibole schist from the Nagaland ophiolite complex, NE India: a look into their metamorphic and tectonic evolution. Int. Geol. Rev., pp. 1-27.

Ao, A., Bhowmik, S. K. and Upadhyay, D. (2020). PT-melt/fluid evolution of abyssal mantle peridotites from the Nagaland Ophiolite Complex, NE India: Geodynamic significance. Lithos, v. 354, pp.105344.

Ao, A. and Bhowmik, S.K. (2014). Cold subduction of the Neotethys: the metamorphic record from finely banded lawsonite and epidote blueschists and associated metabasalts of the Nagaland Ophiolite complex, India. Jour. Metam. Geol., v. 32(8), pp. 829-860.

Bhowmik, S.K. and Ao, A. (2016). Subduction initiation in the Neo-Tethys: constraints from counterclockwise P-T paths in amphibolite rocks of the Nagaland Ophiolite complex, India. Jour. Metam. Geol., v. 34(1), pp. 17-44.

Brunnschweiler, R.O. (1966). On the geology of Indo-Burman Ranges. Jour. Geol. Soc. Australia, v.13.

Blundy, J.D. and Holland, T.J.B. (1990). Calcic amphibole equilibria and a new amphibole-plagioclase geothermometer. Contrib. Mineral Petrol., v. 104, pp. 208-224.

Chakungal, J., Jaroslav, D., Grujic, D., Stephanie, D. and Ghalley, K.S. (2010). Provenance of the Greater Himalayan sequence: Evidence from mafic granulites and amphibolites in NW Bhutan. Tectnophysics, v. 480 (1-4), pp. 198-212.

Chatterjee, N. and Ghose, N.C. (2010). Metamorphic evolution of the Naga Hills eclogite and blueschist, Northeast India: implications for early subduction of the Indian plate under the Burma microplate. Jour. Metam. Geol., v. 28, pp. 209-225.

Corie, S.L., Kohn, M.J. and Vervoort, J.D. (2010). Young eclogite from the Greater Himalayan Sequence, Arun Valley, eastern Nepal: P-T-t path and tectonic implications. Earth Planet. Sci., v.289(3-4), pp. 406-416.

De Sigoyer, J., Chavangnac, V., Blichert T. J., Villa, I.M., Luais, B., Guillot, S., Cosca, M., and Mascle, G. (2000). Dating the Indian continental subduction and collisional thickening in the northwest Himalays: Multichronology of the Tso Morari eclogites. Geology, v. 28, pp. 487-490.

Dilek, Y., Thy, P., Hacker, B and Grundving, S. (1999). Structure and Petrology of Tauride ophiolites and mafic dike intrusions (Turkey): Implications for the Neotethyan ocean. Geol. Soc. Am. Bull., v.111, pp. 1192-1216.

Ellis, D.J. and Green, D.H. (1979). An experimental study of the effect of Ca upon garnet — clinopyroxene Fe-Mg exchange equilibria. Contrib. Mineral Petrol., v. 71, pp.13-22.

Ernst, W.G. and Liu, J. (1998). Experimental phase-equilibrium study of Al- and Ti-contents of calcic amphibole in MORB – a semiquantitative thermobarometer. Am. Mineral., v. 83, pp. 952-969.

Ganguly, J. (1979). Garnet and clinopyroxene solid solutions, and geothermometry based on Fe-Mg distribution coefficient. Geochim. Cosmochim. Acta, v. 43, 1021-1029.

Green, D.H. and Ringwood, A.E. (1967). An experimental invistigation of the gabbro to eclogite transformation and its petrological applications. Geochim. Cosmochim. Acta, v. 31, pp. 767-833.

Greenwood, N.N. and Earnshaw, A. (1998). Chemistry of the elements. 2nd edition, Butterworth-Heinemann, Oxford.

Groppo, C., Rolfo, F. and Castelli, D. (2007) Pre-Alpine HT mineral relics in impure marbles from the UHP Brossasco-Isasca unit (Dora-Maira Massif, western Alps). Periodic. Mineralog., v. 76, pp.155-168.

Groppo, C., Franco, R., Himanshu, S. and Rai, S. (2016). Petrology of blueschist from the western Himalaya (Ladakh, NW India), Exploring the complex behaviour of a lawsonite-bearing system in a paleo-accretionary setting. Lithos, v. 252-253, pp.41-56.

Hacker, B., Mosenfelder, J.L and Edwin Gnos (1996). Rapid emplacement of the Oman ophiolite: Thermal and geochronologic constrainst. Tectonics, v. 15(6), pp. 1230-1247.

Hammarstrom, J.M. and Zen, E. (1986). Aluminium in hornblende: An empirical igneous geobarometer. Am. Mineral., v. 71, pp. 1297-1313.

Holland, T. and Blundy, J. (1994). Non-ideal interactions in calcic amphiboles and their bearing on amphibole-plagioclase thermometry. Contr. Mineral. Petrol., v.116, pp. 433-447.

Holland, T. and Powell, R. (2006). Mineral activity- composition relations

and petrological calculations involving cation equipartition in multisite minerals: A logical inconsistency. Jour. Metam. Geol., v. 24, pp. 851-861.

Hollister, L.S., Grisson, G.C., Peters, E.K., Stowell, H.H. and Sisson, V.B. (1987). Confirmation of the empirical correlation of Al in hornblende with pressure of solidification of calc-alkaline plutons. Am. Mineral., v. 72, pp. 231-239.

Jamieson, R.A. (1986). P-T paths from high temperature shear zones beneath ophiolites. Jour. Metam. Geol., v. 4(1), pp.3-22.

Johnson, M.C. and Rutherford, M.J. (1989). Experimental Calibration of the Aluminium in Hornblende Geobarometer with Application to Long Valley Caldera (California) Volcanic Rocks. Geology, v.17, pp. 837-841.

Kaneko, Y., Katayama, Yamamoto, H., Misawa, K., Ishikawa, M., Rehman, H.U., Kausar, A.B. and Shiraishi, K. (2003). Timing of Himalayan ultrahigh-pressure metamorphism: sinking rate and subduction angle of the Indian continental crust beneath Asia. Jour. Metam.Geol., v. 21(6), pp.589-599.

Khogenkumar, S., Singh, A. K., Kumar, S., Lakhan, N., Chaubey,M., Imtisunep, S., Oinam, G. (2021) Subduction versus non-subduction origin of the Nagaland-Manipur Ophiolites along the Indo-Myanmar Orogenic Belt, northeast India: Fact and fallacy. *Geological Journal*, 56, 1773–1794.

Krogh J. (1988). The garnet-clinopyroxene Fe-Mg geothermometer - a reinterpretation of existing experimental data. Mineral. Petrol., v.99, pp. 44-48.

Liu, J., Cao, S., Zhai, Y., Song, Z., Wang, A., Xiu, Q., Gao, L and Guan, Y. (2007). Rotation of crustal blocks as an explanation of oligo-miocene extension in southeastern Tibet- evidenced by the diancangshan and nearby metamorphic core complexes. Earth Sci. Front., v.14(4), pp. 40-48.

Liou, J.G. (1973) Synthesis and stability relations of epidote, $Ca_2Al_2FeSi_3O_{12}(OH)$. Jour. Geol., v.82, pp.88-97.

Lombardo, B. and Rolfo, F. (2000). Two contrasting eclogite types in the Himalayas: Implications for the Himalayan orogeny. Jour. Geodynam., v. 30(1-2), pp. 37-60.

Mitchell, A., Chung, S.L., Thura, O., Lin, T.H. and Hung, C.H. (2012). Zircon U-Pb ages in Myanmar: Magmatic-metamorphic events and the closure of a neo-Tethys ocean. Jour. Asian Earth Sci., v.66, pp.1-33.

Morimoto, N. et.al. Fabries, J. Ferguson, A.K., Ginzburg, I.V., Ross, M., Seifert, F.A., Zussman, J., Aoki, K. and Gottardi, G. (1988). Nomenclature of pyroxenes. Am. Mineral., v. 73(9-10), pp.525-544.

Mysen, B.O. and Heier, K.S. (1972). Petrogenesis of eclogites in high-grade metamorphic gneisses exemplified by the Hareidland eclogite, west Norway. Contrib. Mineral. Petrol., v.36, pp. 73-94.

Ningthoujam, P.S., Dubey, C.S., Guillot, S., Fagion, A.S. and Shukla, D.P. (2012). Origin and serpentinization of ultramafic rocks of Manipur Ophiolite Complex in the Indo☐ Myanmar subduction zone, Northeast India. Jour. Asian Earth Sci., v.50, pp.128-140.

Pal, T., Bhattacharya, A., Nagendran, G., Yanthan, N.M., Singh, R. and Raghumani, N. (2014). Petrogenesis of chromite from the Manipur ophiolite belt, NE India: Evidence for a supra-subduction zone setting prior to Indo-Myanmar collision. Mineral. Petrol., v.108, pp. 713-726.

Parrish, R.R., Gough, S.J., Searle, M.P. and Waters, D.J. (2006). Plate velocity exhumation of ultrahigh-pressure eclogites in the Pakistan Him. Geol., v.34, pp. 989-992.

Pouchou, J.L. and Pichoir, F. (1985). Quantitative Analysis of Homogeneous or Stratified Microvolumes, Applying the Modal PAP. Electron Probe Quantit., pp. 31-75.

Pradhan, P., Lukose, L., Bhomick, S.K., Sorcar, N., Ranjan, S. and Upadhyay, D. (2022). Early Jurassic Ultra-hot Subduction Zone Metamorphism within the Neo-Tethys: Evidence from High-Temperature Metamorphic Sole rocks in the Nagaland-Manipur Ophiolite Belt, NE India. Goldschmidt Conf.

Raheim, A. and Green, D.H. (1974). Experimental determination of the temperature and pressure dependence of the Fe-Mg partition coefficient for coexisting garnet and clinopyroxene. Contr. Mineral Petrol., v. 48, pp.179-203.

Robertson, A.H.F. (2002) Overview of the genesis and emplacement of Mesozoic ophiolites in the eastern Mediterranean Tethyan region. Lithos, v.65, pp.1-67.

Searle, M.P., Noble, S.R., Cottle, J.M., Waters, D.J., Mitchell, A.H.G., Hlaing, T. and Horstwood, M.S.A., (2007). Tectonic evolution of the Mogok Metamorphic belt, Burma (Myanmar) constrained by U-Th-Pb dating of metamorphic and magmatic rocks. Tectonics, v.26, pp.TC3014.

Schmidt, M.W. (1992). Amphibole composition in tonalite as a function of pressure: An experimental calibration of the Al-in-hornblende barometer. Contrib. Mineral. Petrol., v.110, pp.304-310.

Singh, A.K. (2009). High-Al chromium spinel in peridotites of Manipur Ophiolite Complex, Indo-Myanmar Orogenic Belt: Implication for petrogenesis and geotectonic setting. Curr. Sci., v.96, pp.973-978.

Singh, T.G., and Kom, T.S. (2017). Remote sensing and Photogeology aided Geological Mapping in unmapped terrain in parts of Chandel District, Manipur (Parts of Toposheet 83 L/04 and 84 I/01) on 1:50,000 scale. Unpublished GSI report, FS 2016-17.

Singh, A.K., Nayak, R., Khogenkumar, S., Subramanyam, K.S.V., Thakur, S.S., Bikramaditya Singh, R.K. and Satyanarayanan, M. (2017). Genesis and tectonic implications of cumulate pyroxenites and tectonite peridotites from the Nagaland-Manipur ophiolites, Northeast India: Constraints from mineralogical and geochemical characteristics. Geol. Jour., v.52, pp.415-436.

Tsujimori, T. and Harlow, G.E. (2012). Petrogenetic relationships between jadeitite and associated high-pressure and low-temperature metamorphic rocks in worldwide jadeitite localities: a review. Europ. Jour. Mineral., v. 24, pp.371-390.

Williams, H. and Smyth, W.R. (1973). Metamorphic aureoles beneath ophiolite suites and alpine peridotites: tectonic implications with west New-Foundland examples. Am. Jour. Sci., v.*273*(7), pp.594-621. https://doi.org/10.2475/ajs.273.7.594

Wolf, M.B. and Wyllie, P.J. (1993). Garnet growth during amphibolite anatexis: implications of a garnetiferous restate. Jour. Geol., v.101, pp.353-373.

Zhang, J., Xiao, W., Windley, Braian F., Fulong, C., Sein, K., Naing, S. (2017). Early Cretaceous wedge extrusion in the Indo-Burma Range accretionary complex: implications for the Mesozoic subduction of Neothys in SE Asia. International Jour. Earth Sci., v. 106(4), pp. 1391-1408.

Zhang, J., Chunjing, W. and Hang, C. (2018). Multiple metamorphic events recorded in the metamorphic terranes in central Inner Mongolia, Northern China: Implication for the tectonic evolution of the Xingian -Inner Mongolia Orogenic Belt. Jour. Asian Earth Sci., v.167, pp. 52-67.